Synthesis and Characterization of Dimeric Mutually Coordinated Magnesium *meso*-2-Pyridylporphyrins

Nikolay N. Gerasimchuk, Andrew A. Mokhir, and Kenton R. Rodgers*

Department of Chemistry, North Dakota State University, Fargo, North Dakota 58105

Received November 11, 1997

The synthesis and characterization of a series of *meso*-2-pyridylporphyrins and their Mg^{2+} complexes are reported. Condensation of 4-alkylbenzyl-2,2′-dipyrromethanes (alkyl = Me, *n*-Pr, or *n*-Bu) with 2-pyridinecarboxaldehyde yielded a series of free-base *meso*-2-pyridylporphyrins. Insertion of Mg^{2+} into the free-base porphyrins yielded the respective magnesium complexes. These compounds were characterized using 1D (^{1}H and ^{13}C) and 2D (^{1}H−^{1}H COSY) NMR methods, UV−visible absorption spectroscopy, fluorescence spectroscopy, and mass spectrometry. The interplanar spacing of the dimers is sufficiently small that there is excitonic coupling of the constituent chromophores. The overall dissociation constant of these dimers is estimated at 2×10^{-6} M. Addition of donor ligands such as acetone, DMF, DMSO, or pyridine converts the dimeric species to their respective constituent monomers. Titration of the dimeric complex with pyridine-d_5 shows that disaggregation requires coordination of two pyridine molecules at independent binding sites. Tracking of the pyridine coordination by ^{1}H NMR spectroscopy allowed for determination of the equilibrium constant for the pyridine-induced disaggregation reaction (2.1×10^{-3} M^2). Both the spontaneous dissociation and the pyridine-induced disaggregation reactions occur by two steps.

Introduction

Tetrapyrrolic chromophores are ubiquitous in nature as free-base porphyrins and chlorins and as metal ion complexes. The metal ion complexes fulfill a variety of roles, including oxygen storage, transport, and sensing, oxygen activation, electron transfer, light harvesting, and energy transfer. Interactions between tetrapyrrolic chromophores play important roles in biological energy and electron-transfer processes.[1−3] The nature of these interactions is dictated by the distance between the chromophores, their relative orientations, and their redox potentials.[4,5] One chromophore−chromophore interaction that has been the subject of intense investigation is that of the special pair of bacteriochlorophylls in the bacterial photoreaction centers.[1,4] The bacteriochlorophyll planes in these dimeric complexes are in a closely spaced cofacial edge-over-edge arrangement, which puts their π systems in van der Waals contact with one another. Their metal centers are laterally displaced such that a peripheral formyl group can coordinate to the Mg^{2+} center of the partner bacteriochlorophyll.[4,5] A number of porphyrin and chlorin complexes with this type of structure have been investigated.[6] The electronic consequences of these structural features are that (1) in-plane electronic transitions having large oscillator strengths are split due to excitonic interaction between the chromophores[6] and (2) charge-resonance transitions having moments with interplanar components are often observed.[7] Hence, this structural motif provides a design platform for assembly of well-characterized chromophores into aggregates having ground and excited states that are distinct from those of the constituent monomers and that are accessible by absorption of UV, visible and near-IR light.[8] Insofar as the energies and molar absorptivities of these aggregates can be tuned by judicious synthetic design, this class of complexes may find use as nonlinear optical and/or light-harvesting materials.[8]

Studies of the complexes in this class have been largely concerned with demonstration of structure.[6] To date, the

* To whom correspondence should be addressed. Phone: 701-231-8746. Fax: 701-231-8831. E-mail: rodgers@plains.nodak.edu.

(1) (a) Bowler, B. E.; Raphael, A. L.; Gray, H. B. *Prog. Inorg. Chem.* **1990**, *38*, 259−322. (b) McClendon, G. *Acc. Chem. Res.* **1988**, *21*, 160. (c) Hoffmann, B. M.; Ratner, M. A. *J. Am. Chem. Soc.* **1987**, *109*, 6237−6243.
(2) Heller, B. A.; Holten, D.; Kirmaier, C. *Science* **1995**, *262*, 940.
(3) Berg, A.; Rachamim, M.; Galili, T.; Levanon, H. *J. Phys. Chem.* **1996**, *100*, 8791−8795.
(4) Deisenhofer, J.; Michel, H. *Science* **1989**, *245*, 1463−1473.
(5) (a) Deisenhofer, J.; Epp, O.; Miki, K.; Huber, R.; Michel, H. *J. Mol. Biol.* **1984**, *180*, 385−398. (b) Allen, J. P.; Feher, G.; Yeates, T. O.; Komiya, H.; Rees, D. C. *Proc. Natl. Acad. Sci. U.S.A.* **1987**, *84*, 5730−5734.
(6) (a) Kobuke, Y.; Miyaji, H. *J. Am. Chem. Soc.* **1994**, *116*, 4111−4112. (b) Stibrany, R. T.; Vasuderan, J.; Knapp, S.; Potenza, J. A.; Emge, T.; Schugar, H. J. *J. Am. Chem. Soc.* **1996**, *118*, 3980−3981. (c) Munro, O. Q.; Marques, H. M. *Inorg. Chem.* **1996**, *35*, 3768−3779. (d) Tran-Thi, T. H.; Lipskier, J. F.; Maillard, P.; Momenteau, M.; Lopez-Castillo, J.-M.; Jay-Gerin, J.-P. *J. Phys. Chem.* **1992**, *96*, 1073−1082. (e) Senge, M. O.; Vicente, M. G. H.; Gerzevske, K. R.; Forsythe, T. P.; Smith, K. M. *Inorg. Chem.* **1994**, *33*, 5625−5638. (f) Clement, T. E.; Murco, D. J.; Smith, K. M. *Inorg. Chem.* **1998**, *37*, 1150−1160. (g) Chernook, A. V.; Shulga, A. M.; Zenkevich, E. I.; Rempel, U.; Borczyskowski, C. V. *J. Phys. Chem.* **1996**, *100*, 1918−1926. (h) Bucks, R. R.; Boxer, S. G. *J. Am. Chem. Soc.* **1982**, *104*, 340−343. (i) Ohno, O.; Kaizu, Y.; Kobayashi, H. *J. Chem. Phys.* **1993**, *99*, 4128−4139. (j) Kaizu, Y.; Maekawa, H.; Kobayashi, H. *J. Phys. Chem.* **1986**, *90*, 4243−4238.
(7) (a) Gottfried, D. S.; Steffen, M. A.; Boxer, S. G. *Science* **1991**, *251*, 662−665. (b) Bilsel, O.; Rodriguez, J.; Milam, S. N.; Gorlin, P. A.; Girolami, G. S.; Suslick, K. S.; Holten, D. *J. Am. Chem. Soc.* **1992**, *114*, 6528−6538. (c) Ohno, O.; Ishikawa, N.; Matsuzawa, T.; Kobayashi, H. *J. Phys. Chem.* **1989**, *93*, 1713−1718. (d) Petke, J. D.; Maggiora, G. M. *J. Chem. Phys.* **1986**, *84*, 1640−1652. (e) Thompson, M. A.; Zerner, M. C.; Fajer, J. *J. Phys. Chem.* **1990**, *94*, 3820−3828. (f) Thompson, M. A.; Zerner, M. C.; Fajer, J. *J. Phys. Chem.* **1991**, *95*, 5693−5700.
(8) Perry, J. W.; Mansour, K.; Lee, I.-Y. S.; Wu, X.-L.; Bedworth, P. V.; Chen, C.-T.; Ng, D.; Marder, S. R.; Miles, P.; Wada, T.; Tian, M.; Sasabe, H. *Science* **1996**, *273*, 1533−1536.

10.1021/ic971421t CCC: $15.00
Published on Web 10/02/1998

Scheme 1

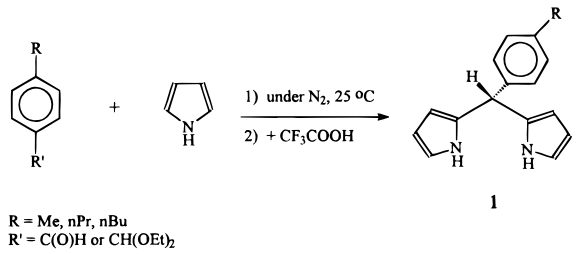

chemistry of aggregation and disaggregation remains unreported. Herein, we describe the synthesis and characterization of new dimeric magnesium tetraarylporphyrin complexes containing peripheral *meso*-2-pyridyl substituents, which facilitate mutual coordination between monomers. We demonstrate that the complexes are dimeric in solution with the porphyrin ligands overlapping at one edge in a closely spaced cofacial arrangement. UV−visible, NMR, and fluorescence data indicate that these complexes are stable in 10^{-4} M solution. Additionally, thermodynamic stabilities of the dimeric complexes and the nature of their dissociation and pyridine-induced disaggregation reactions are reported.

Experimental Section

General Considerations. All reagents were received 96−99% pure and were used without further purification. Trace amounts of HCl were removed from CH_2Cl_2 and $CHCl_3$ immediately before use by passing them through a small column containing layers of anhydrous Na_2CO_3 and Na_2SO_4. Toluene, C_2H_5OH, acetonitrile, and methanol were reagent grade and were not purified further. Acetone and pyridine were dehydrated using activated 3-Å molecular sieves.

Synthetic Methods. Syntheses of *meso*-2-pyridylporphyrins were accomplished in two steps. The first was preparation of dipyrromethanes by the method of Lee and co-workers[9] (Scheme 1). The second was reaction of the dipyrromethanes with 2-pyridinecarboxaldehyde. This reaction yielded the porphyrin products shown in Scheme 2. Table 1 shows the abbreviation scheme for the reported compounds; these abbreviations are used throughout. A reactant stoichiometry of 1:1 was used throughout the syntheses, as it favored formation of the monosubstituted *meso*-2-pyridylporphyrins, 3MeH and 3BuH, and *meso*-5,15-bis-2-pyridylporphyrins, 4MeH and 4BuH through the Rothemund-type condensation.[10,11] Excess pyridinecarboxaldehyde resulted in higher yields of the respective *tris*- and *tetrakis*-2-pyridylporphyrins.[12,13]

a. (4-Methylphenyl)dipyrromethane, 1Me. At room temperature under N_2 flow in a two-neck flask, 10 mL (0.14 M) of neat pyrrole and 0.4 mL (3.4 mM) of 4-methylbenzaldehyde (or an equimolar amount of the corresponding dimethyl- or diethylacetal) were mixed. After the mixture was purged for 20 min, a catalytic amount of CF_3-COOH (20 mL) was added with stirring. Consumption of the starting aldehyde was monitored by TLC. After ∼1 h, the reaction mixture was diluted with 20 mL of CH_2Cl_2 and washed twice with 20 mL of 0.1 M NaOH. The slightly yellow organic layer was dried over Na_2-SO_4. Dichloromethane was removed by rotary evaporation, and excess pyrrole was removed under vacuum (0.016 Torr) at 50 °C for ∼10 h to give 0.75 g (93%) of a yellow-brown waxy solid. The 1Me thus isolated was ∼85% pure and was used for the Rothemund condensation (Scheme 2) without further purification. ^{1}H NMR chemical shifts (ppm): 2.41 [3H] singlet, CH_3−; 5.43 [1H] singlet, methane proton; 5.97 [2H] multiplet, γ-pyrrole; 6.21 [2H] multiplet, β-pyrrole; 6.67 [2H] multiplet, α-pyrrole; 7.16 [4H] multiplet, phenyl; 7.84 [∼2H] broadened singlet, pyrrole NH.

Scheme 2

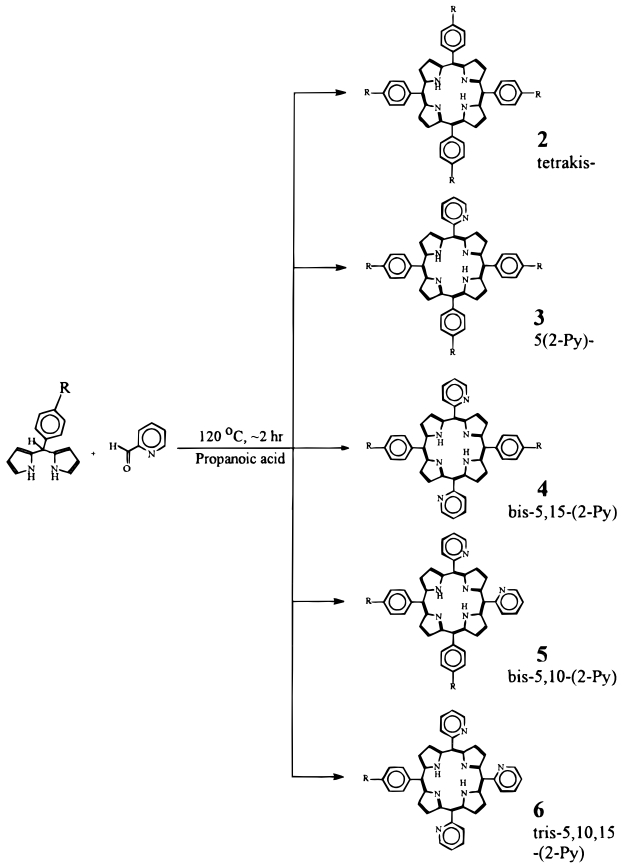

Table 1. Compounds Synthesized and Characterized in This Study

compd type	*meso*-4-phenyl substituent	porphyrin core	compd designation	*n* (from Scheme 2)
dipyrromethane	Me		1Me	
dipyrromethane	*n*Pr		1Pr	
dipyrromethane	*n*Bu		1Bu	
free-base porphyrin	Me	$2H^+$	*n*MeH	2, 3, 4, 5, 6
free-base porphyrin	*n*Pr	$2H^+$	*n*PrH	2, 3, 4
free-base porphyrin	*n*Bu	$2H^+$	*n*BuH	2, 3, 4, 5, 6
metalloporphyrin	Me	Mg^{2+}	*n*MeMg	2, 3 & 4
metalloporphyrin	*n*Pr	Mg^{2+}	*n*PrMg	3
metalloporphyrin	*n*Bu	Mg^{2+}	*n*BuMg	2, 3, 4

b. (4-Propylphenyl)dipyrromethane, 1Pr, and (4-Butylphenyl)-dipyrromethane, 1Bu. These dipyrromethanes were prepared in a manner analogous to that described for 1Me. However, purification of the crude product was necessary. The dark-yellow residue obtained from the condensation reaction was redissolved in 15 mL of a 1:1 EtOAc/cyclohexane mixture, loaded onto a 3 × 30 cm^2 SiO_2 column, and eluted using a mixture of ethyl acetate(10%), cyclohexane (89%), and triethylamine (1%). The second band contained 0.58 g (57%) of pure, pink-yellow dipyrromethane. Removal of solvent by rotary evaporation yielded a waxy solid. ^{1}H NMR chemical shifts for 1Bu (ppm): 0.97 [3H] triplet, *n*-Bu; 1.39 [2H] sextet, *n*-Bu; 1.62 [2H] quintet, *n*-Bu; 2.62 [2H] triplet, benzyl; 5.43 [1H] singlet, methane proton; 5.94 [2H] multiplet, γ-pyrrole; 6.17 [2H] β-pyrrole; 6.66 [2H] multiplet, α-pyrrole; 7.14 [4H] multiplet, phenyl; 7.85 [∼2H] broad singlet, NH pyrrole.

^{13}C NMR spectra of both dipyrromethanes, 1Me and 1Bu, can be found in Supporting Information (Figures S1 and S2).

(9) Lee, C.-H.; Lindsey, J. S. *Tetrahedron* **1994**, *50*, 11427−11440.
(10) Rothemund, P. *J. Am. Chem. Soc.* **1935**, *57*, 2010.
(11) Fisher, H.; Orth, H. *Die Chemie des Pyrrols*; Academische Verlagsgesellshaft: Leipzig, 1937; Vol. II.
(12) Kobayashi, N. *Inorg. Chem.* **1985**, *24*, 3324.
(13) (a) Kim, J. B.; Adler, A. D.; Longo, F. R. In *The Porphyrins*; Dolphin, D., Ed.; Academic Press: New York, 1978; Vol. 1, Chapter 3. (b) Little, R. G.; Anton, J. A.; Loach, P. A.; Ibers, J. A. *J. Heteromet. Chem.* **1975**, *12*, 343.

Table 2. Absorption Maxima for Mg(II) and Zn(II) Porphyrins[a]

compd	Q(0,0)	Q′(0,0)	Q″(0,0)	Q(0,1)	B(0,0)	B′(0,0)	B″(0,0)	ref
Mg(TPP)	602			563	426			33
2BuMg	603			564	427			*b*
3BuMg	605			564	426			*b*
$[3MeMg]_2$		617 (3.36)	603	568 (4.02)		430 (5.00)	414 (5.05)	*b*
$[3BuMg]_2$		617 (3.97)	603	568 (4.27)		429 (5.19)	414 (5.26)	*b*
3BuMg(py)	613			570	430			*b*
$\{Zn[(2\text{-MeIm})OEP]\}_2$	591			556		426	408	6a
$\{Zn[(2\text{-py})Tr(t\text{-BuP})P]\}_2$		614	565	526		432	416	6b

[a] Values in parentheses are log $\epsilon_{\lambda max}$ per monomer. [b] This work.

c. General Synthesis of *meso*-2-Pyridylporphyrins. Reactions of 2-pyridinecarboxaldehyde with the aforementioned dipyrromethanes were carried out in 100 mL of propionic acid under reflux conditions. The reactions were monitored by UV−visible absorption and were complete within 3 h. When the reaction was complete, the flask was cooled in an ice bath and the mixture was diluted with 150 mL of water. Aqueous ammonia (∼35%) was added dropwise with stirring to neutralize the acid. At pH 7−8, the porphyrins were extracted with 3 × 20 mL of CH_2Cl_2. The resulting dark-purple organic layer was dried over anhydrous Na_2SO_4 and plug-filtered through neutral Al_2O_3. The CH_2Cl_2 solution of porphyrins was concentrated and loaded onto an SiO_2 column. Stepwise increases in the methanol content of the dichloromethane eluent from 1% to 10% allowed separation of the five porphyrins shown in Scheme 2.

d. Porphyrins 2MeH−6MeH. Using this procedure, 1Me and 2-pyridinecarboxaldehyde were reacted to give porphyrins 2MeH−6MeH with an overall yield of 33%. Spectroscopic data for these compounds are given below. ^1H and ^{13}C NMR data are available upon request.

d.1. *meso*-(Tetrakistolyl)porphyrin, 2MeH [Mg(TTP)]. Yield: ∼30 mg (∼3%). R_f = 0.93 (cyclohexane/EtOAc = 1:1). Visible absorbance: λ_{max} (nm) = 421.9, 518.9, 555.0, 596.5, 652.9.

d.2. *meso*-2-Pyridyltristolylporphyrin, 3MeH. Yield: 180 mg (∼17%). R_f = 0.75 (cyclohexane/EtOAc = 1:1). Visible absorbance: λ_{max} (nm) = 421.7, 518.9, 556.5, 596.5, 652.2. Mass-spectrometry data for $C_{46}H_{35}N_5$: calcd 657.8, found, 658.1 = M + 1.

d.3. *meso*-(5,15-Bis{2-pyridyl}-10,20-bistolyl)porphyrin, 4MeH. Yield: ∼100 mg (∼10%). R_f = 0.63 (cyclohexane/EtOAc = 1:1). Visible absorbance: λ_{max} (nm) = 421.3, 517.9, 554.3, 595.8, 652.6. Mass-spectrometry data for $C_{44}H_{32}N_6$: calcd 644.8, found, 645.3 = M + 1.

d.4. *meso*-(5,10-Bis-{2-pyridyl}-15,20-bistolyl)porphyrin, 5MeH. Yield: ∼20 mg (∼2%). R_f = 0.21 (cyclohexane/EtOAc = 1:1) or 0.60 (cyclohexane/acetone = 1:1). Visible absorbance: λ_{max} (nm) = 422.2, 517.9, 595.0, 650.9. Mass-spectrometry data for $C_{44}H_{32}N_6$: calcd 644.8, found, 645.3 = M + 1.

d.5. *meso*-(Tris-{2-pyridyl}tolyl)porphyrin, 6MeH. Yield: ∼20 mg (∼2%). R_f = 0.36 (cyclohexane/acetone = 1:1). Visible absorbance: λ_{max} (nm) = 421.3, 517.1, 522.6, 595.0, 651.7. Mass-spectrometry data for $C_{42}H_{29}N_7$: calcd 631.7, found (632.4 = M + 1.

e. Porphyrins 2BuH−6BuH. Reaction of 1Bu with 2-pyridinecarboxaldehyde yielded free-base ligands 2BuH−6BuH with an overall yield of 50%. Spectroscopic data for these compounds are given below. ^1H and ^{13}C NMR data are available upon request.

e.1. *meso*-(Tetrakis-{4-*n*-butylphenyl})porphyrin, 2BuH. Yield: ∼15 mg (<2%). R_f = 0.94 (cyclohexane/EtOAc = 4:1). Visible absorbance: λ_{max} (nm) = 421.2, 519.3, 555.8, 597.4, 657.5. Mass-spectrometry data for $C_{60}H_{62}N_4$: calcd 839.2, found 840.0 = M + 1). $C_{60}H_{62}N_4{*}H_2O$: calcd 856.2, found 856.0.

e.2. *meso*-({2-Pyridyl}-[tris-{4-*n*-butylphenyl}])porphyrin, 3BuH. Yield: 120 mg (∼15%). R_f = 0.85 (cyclohexane/EtOAc = 1:1). Visible absorbance: λ_{max} (nm) = 420.8, 518.4, 554.3, 597.6, 658.2. Mass-spectrometry data for $C_{55}H_{53}N_5$: calcd 784.0, found 784.9 = M + 1). $C_{55}H_{53}N_5{*}H_2O$: calcd 802.0, found 801 = M′ − 1.

e.3. *meso*-(5,15-Bis-{2-pyridyl}-[10,20-bis-{4-*n*-butylphenyl}])-porphyrin, 4BuH. Yield: 230 mg (28%). R_f = 0.73 (cyclohexane/EtOAc = 1:1) and 0.19 (cyclohexane/EtOAc = 4:1). Visible absorbance: λ_{max} (nm) = 420.3, 517.4, 553.2, 596.8, 658.5. Mass-spectrometry data for $C_{50}H_{44}N_6$: calcd 728.9, found 729.8 = M + 1.

e.4. *meso*-(5,10-Bis-{2-pyridyl}-[15,20-bis-{4-*n*-butylphenyl}])-porphyrin, 5BuH. Yield: 30 mg (<4%). R_f = 0.22 (cyclohexane/EtOAc = 1:1) and 0.59 (cyclohexane/acetone = 1:1). Visible absorbance: λ_{max} (nm) = 419.7, 516.2, 551.4, 594.8, 650.3.

e.5. *meso*-(Tris-{2-pyridyl}-{4-*n*-butylphenyl})porphyrin, 6BuH. Yield: ∼15 mg (<2%). R_f = 0.46 (cyclohexane/acetone = 1:1). Visible absorbance: λ_{max} (nm) = 419.2, 517.4, 553.2, 594.6, 656.8.

e.6. *meso*-(Tetrakis-{4-*n*-propylphenyl})porphyrin, 2BuH, *meso*-({2-Pyridyl}-[tris-{4-*n*-propylphenyl}])porphyrin, 3BuH, *meso*-(5,-15-Bis-{2-pyridyl}-[10,20-bis-{4-*n*-propylphenyl}])porphyrin, 4BuH, *meso*-(5,10-Bis-{2-pyridyl}-[15,20-bis-{4-*n*-propylphenyl}])-porphyrin, 5BuH, and *meso*-(Tris-{2-pyridyl}-{4-*n*-propylphenyl})-porphyrin, 6BuH. The synthesis, purification, yields, and spectral properties of these *meso*-4-*n*-propylphenylporphyrins were analogous to those of the *meso*-4-*n*-butylphenyl derivatives described above.

f. Synthesis of Magnesium Porphyrin Complexes. Insertion of Mg^{2+} was carried out according to literature procedures.[15] Molar absorptivities were determined for 3MeMg and 3BuMg and are given in Table 2. Although molar absorptivities were not carefully determined for the other Mg^{2+} complexes, they were observed to lie within the range of typical magnesium tetraarylporphyrins.[14]

f.1. Mg[*meso*-{tetrakistolyl}porphyrin], 2MeMg. Purple solid. R_f = 0.62 (cyclohexane/EtOAc = 4:1). Visible absorbance, in CH_2Cl_2, 0.1 mm cell: λ_{max} (nm) = 402.5, 423.1, 562.3, 602.8. Proton NMR ($CDCl_3$; 64 scans) chemical shifts, ppm: 8.85 [8H] singlet, b-pyrrole; 8.09 [8H] doublet, tolyl; 7.51 [8H] doublet, tolyl; 2.69 [12H] singlet, CH_3 tolyl.

f.2. Mg[*meso*-({2-pyridyl}-tristolyl)porphyrin], 3MeMg. Green solid. R_f = 0.66 (cyclohexane/EtOAc = 1:1). Visible absorbance, in CH_2Cl_2, 0.1 mm cell: λ_{max} (nm) = 410.6, 427.1, 567.0, 605, 614. Mass-spectrometry data for $C_{46}H_{33}N_5Mg$: calcd 680.1, found 680.2. Dimer: calcd 1360.2, found 1360.5. Monomer/dimer = 13:1.

f.3. Mg[*meso*-(5,15-bis-{2-pyridyl}-10,20-bistolyl)porphyrin], 4MeMg. Dark-brown solid. R_f = ∼0.3 (cyclohexane/EtOAc = 1:1). Visible absorbance, in CH_2Cl_2, 0.1 mm cell: λ_{max} (nm) = 411.2, 427.0, 565.6, 615.3. Mass-spectrometry data for $C_{44}H_{30}N_6Mg$: calcd (667.1, found 667.2. Dimer and trimer, respectively: calcd 1334.1, found 1334.5 and calcd 2001.2, found 2001.8.

f.4. Mg[*meso*-(tetrakis-{4-*n*-butylphenyl})porphyrin], 2BuMg. R_f = 0.75 (cyclohexane/EtOAc = 4:1). Visible absorbance, in CH_2Cl_2, 0.1 mm cell: λ_{max} (nm) = 407.2, 429.4, 559.2, 609.7.

f.5. Mg[*meso*-({2-pyridyl}-tris-{4-butylphenyl})porphyrin], 3BuMg. Red-purple solid. R_f = 0.75 (cyclohexane/EtOAc = 1:1). Visible absorbance, in CH_2Cl_2, 0.1 mm cell: λ_{max} (nm) = 415.3, 429.2, 569.1, 605, 618. Mass-spectrometry data for $C_{55}H_{51}N_5Mg$: calcd 806.3, found 806.4. Dimer: calcd 1612.6, found 1611.8. Monomer/dimer = 8.6:1.

f.6. Mg[*meso*-(5,15-bis-{2-pyridyl}-10,20-bis-{4-*n*-butylphenyl})-porphyrin], 4BuMg. Dark-blue-purple solid. R_f = 0.43 (cyclohexane/EtOAc = 1:1). Visible absorbance, in ethyl acetate, 0.1 mm cell: λ_{max} (nm) = 427.2, 567.3, 608.7. Mass-spectrometry data for $C_{50}H_{42}N_6$-Mg: calcd 751.2, found 752.5 = M + 1.

(14) Gouterman, M. In *The Porphyrins*; Dolphin, D., Ed.; Academic Press: New York, 1978; Vol. III, Chapter 1.
(15) Lindsey, J. S.; Woodford, J. N. *Inorg. Chem.* **1995**, *34*, 1063−1069.

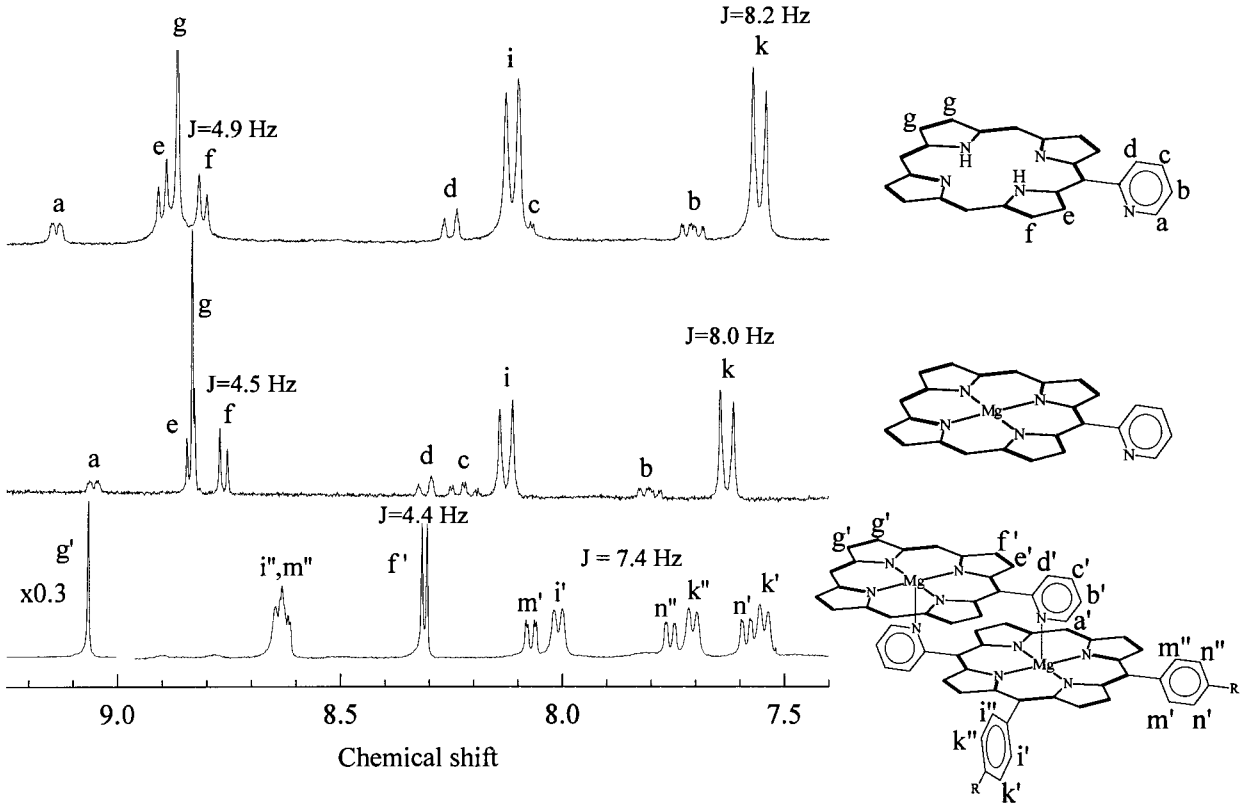

Figure 1. Typical ^{1}H NMR spectra of the indicated *meso*-2-pyridylporphyrins. The remaining meso positions are occupied by *p*-alkylphenyl substituents. These groups are omitted from the top two structures for the sake of clarity. One of each type of phenyl group is included in the dimer structure to clarify the labeling scheme. Top: 3BuH in $CDCl_3$. Middle: monomeric 3BuMg in acetone-d_6. Bottom: dimeric 3BuMg in $CDCl_3$. Assignments are based on COSY experiments for the free-base and metal complexes (see Supporting Information).

The synthesis, purification, and spectral properties of the *meso*-4-*n*-propylphenylporphyrin complexes were analogous to those of the *meso*-4-*n*-butylphenylporphyrin complexes described in the preceding section.

Physical Measurements. UV−visible, IR, and fluorescence spectra were recorded using commercial instruments. Infrared spectra of the reported compounds were obtained from KBr pellets. Fluorescence spectra of Mg porphyrinates were obtained using 413-nm excitation in the front-face illumination mode.

Proton NMR spectra for dipyrromethanes, free-base porphyrins and magnesium porphyrins were recorded in $CDCl_3$ solution at 290 K at 270 or 400 MHz. Carbon-13 spectra (recorded at 100 MHz) and all ^{1}H COSY (recorded at 400 MHz) data were obtained from $CDCl_3$ solutions at ambient temperature.

Mass-spectrometric studies of the porphyrins 2MeH−6BuH were conducted using positive FAB method (using *m*-nitrobenzyl alcohol, NBA, as the matrix). Electrospray ionization was employed for studies of Mg complexes 3MeMg, 4MeMg, 3BuMg, and 4BuMg to facilitate detection of molecular ions for the dimeric complexes.

Results & Discussion

Free-Base Porphyrins. The free-base porphyrin ligands shown in Scheme 2 yield ^{1}H NMR spectra in which the chemical shifts of protons in similar chemical environments cluster in narrow frequency regions. For example, the β-pyrrole and *meso*-aryl (i.e., 4-alkylphenyl and 2-pyridyl) ^{1}H NMR signals in the spectra of the various 2-pyridyl-substituted tetraarylporphyrins differ primarily in their relative intensities and splitting patterns (see Supporting Information for ^{1}H NMR spectra), but the chemical shift differences between protons in analogous environments of the various porphyrins are small. Assignments of the ^{1}H resonances of the free-base porphyrins are based on ^{1}H−^{1}H COSY experiments (Supporting Information, Figure S3). These assignments are indicated in Figure 1 using the labeling scheme shown on the porphyrin skeleton structures.

Structure of the Porphyrin Aggregates in Solution. Electrospray ionization mass spectral analysis of 3MeMg and 4MeMg revealed the presence of molecular ions for both monomer and dimer. The mass spectra indicate significant amounts of monomeric porphyrins ($3MeMg/[3MeMg]_2 = 8.6$ and $4MeMg/[4MeMg]_2 = 13$). It is unclear whether the dimers are largely disaggregated during ionization or by exposure to HCl (which disaggregates the dimers) that accumulated in the $CHCl_3$ solvent during shipping to the mass-spectrometry lab. Although these data do not allow quantitation of solution species, the mass spectra suggest the presence of $[3MeMg]_2$ and $[4MeMg]_2$ in noncoordinating solvents. It should be noted that the dimers observed in the mass spectrum could be due to stability associated with their positive charge, as has been observed for uncoordinated cofacial metalloporphryins in solution and in the solid state.[16]

The ^{1}H NMR spectra of the free-base porphyrin ligands and their respective monomeric magnesium complexes in solvents such as acetone and DMSO are similar (Figure 1). However, spectra of concentrated magnesium porphyrin solutions in $CDCl_3$ or CD_2Cl_2 differ substantially from those obtained in acetone solution (Figure 1). The spectrum of concentrated 3BuMg in $CDCl_3$ has been assigned by ^{1}H−^{1}H COSY (Supporting Information, Figures S4−S6). The most striking features of the spectrum are the marked upfield shifts of (a) two of the four β-pyrrole protons and (b) those on the *meso*-2-pyridyl group. Selective shielding of the *meso*-2-pyridyl protons and the adjacent β-pyrrole protons suggests that they lie within the

(16) Scheidt, R. W.; Lee, Y. J. *Structure and Bonding*; **1987**, *64*, 1−70.

shielding zone of another porphyrin ring.[17] The remarkable 6.57-ppm upfield shift of the a′ proton (α to the pyridyl nitrogen) further suggests that it is held deep within the shielding zone of a partner porphyrin by coordination of the pyridyl nitrogen to the magnesium ion of the shielding porphyrin.[6b,17,18] The b′, c′, and d′ resonances are also shifted upfield by the porphyrin ring current (−1.7, −1.49, and −2.39 ppm, respectively) due to proximity of the 2-pyridyl substituent to the face of a partner porphyrin. These resonances are sharp and exhibit the same coupling patterns as their free-base counterparts.

In the ^{1}H NMR spectra of the free-base porphyrins and their Mg^{2+} complexes, the *β*-pyrrole proton intensity is distributed between three signals. The first is a singlet (g, g′), which actually arises from two chemically inequivalent protons whose chemical shifts differ by less than their coupling constant. The others are two doublets (e, e′ and f, f′). The relative intensities of these signals are 2:1:1 in 3MeH, 3PrH, 3BuH, 3MeMg, 3PrMg, 3BuMg, $[3MeMg]_2$, $[3PrMg]_2$, and $[3BuMg]_2$. This pattern indicates that the plane of symmetry (containing the center of the porphyrin core and the 5-meso carbon) in the free-base porphyrinates is preserved in both monomeric and aggregated Mg complexes. In spectra of the aggregates, the e′ and f′ resonances are sharp Lorentzian doublets, which occur upfield from their free-base counterparts by 3.22 and 0.50 ppm, respectively. The 2-pyridyl and *β*-pyrrole ^{1}H resonances are consistent with formation of a centrosymmetric aggregate that (a) contains one monomer environment, (b) has the porphyrin rings of the constituent monomers partially overlapping, and (c) has the *meso*-2-pyridyl group deep within the ring-current shielding zone of another porphyrin. These structural features coincide with those for a mutually coordinated dimer that is linked through coordination of one porphyrin's *meso*-2-pyridyl group to the Mg center of its partner.

The close proximity of the porphyrin rings in these complexes causes splitting of the 4-alkylphenyl proton signals (Figure 1). Since these groups do not undergo free rotation at ambient temperature,[19] the shielding anisotropy due to ring currents of the partner porphyrin and the coordinated 2-pyridyl groups gives rise to the eight distinct phenyl proton environments shown in Figure 1 (i′, i″, k′, k″, m′, m″, n′, and n″). The phenyl protons oriented toward and away from the partner porphyrin are indicated by ″ and ′, respectively. These resonances have been assigned on the basis of chemical shifts, relative intensities, and the cross-peaks in the COSY map (Supporting Information, Figure S6). Additionally, the m and n assignments in the dimer are clarified by their four-bond J couplings (J_{4m} = 2.0 Hz, J_{4n} = 1.6 Hz). Since the mutually coordinated dimers are centrosymmetric, there are four equivalent *meso*-4-alkylphenyl groups at the 10- and 20-meso positions and two equivalent group at the 15-meso position (across the porphyrin rings from the 2-pyridyl groups). Therefore, the i/m and k/n intensity ratios are 2:1 (Figure 1). The i″ protons lie in the ring-current deshielding zones of both porphyrin rings and consequently are shifted to 8.65 ppm (Figure 1). Similarly, the m″ protons are in the ring-current deshielding zones of their own porphyrin rings and that of the coordinated 2-pyridyl rings of the partner porphyrins. The k″ and n″ protons are deshielded by the same mechanisms but to a lesser extent.

Scheme 3

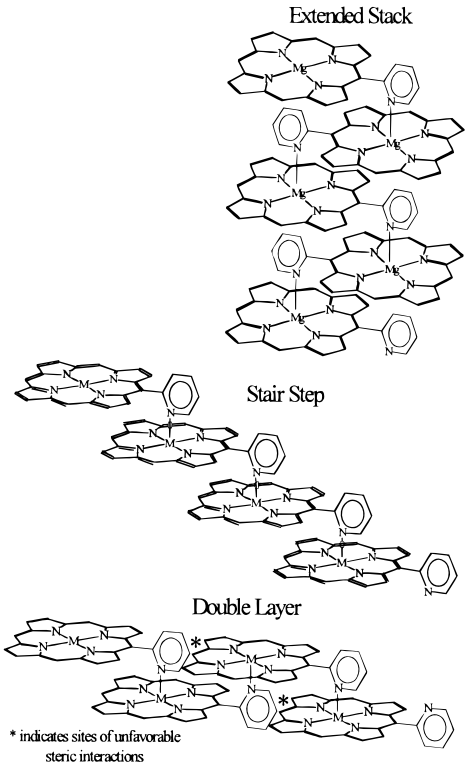

Neither the chemical shifts nor the relative intensities of the resonances in Figure 1 are perturbed significantly by changes in temperature between −50 and 90 °C. However, at elevated temperatures, the i′, i″, k′, and k″ resonances are broadened to the extent that coupling information is lost. Since these are the only resonances that are broadened, introduction of thermal energy increases intradimer steric interactions between the 10- and 20-*meso*-phenyl groups. These temperature-intensified interactions between phenyl groups modulate the chemical environments of the i′, i″, k′, and k″ protons by moving them in and out of each other's shielding and deshielding zones. These chemical shifts, coupling patterns, and temperature dependencies for the *meso*-4-alkylphenyl substituents, together with the intensities and chemical shifts of the *β*-pyrrole and 2-pyridyl proton resonances, are unmistakable signatures of the mutually coordinated dimeric structure shown at the bottom right of Figure 1 (also, see Supporting Information, Figure S6).

A number of structures containing singly linked magnesium 2-pyridylporphyrins in extended stacks, stair-step, and/or two-layer conformations can be visualized and are illustrated in Scheme 3. The NMR spectra of such oligomers could be broadened beyond detection due to the effects of slow tumbling or intermediate site-exchange rates on correlation time (τ_c). However, all *β*-pyrrole proton intensity in the spectrum of a 10^{-3} M $[3PrMg]_2$ solution is accounted for after complete conversion of the dimer to the monomeric pyridine adduct. Complete disaggregation was verified by the UV−visible absorption spectrum. Hence, the possibility of large molecular weight aggregates with peaks too broad to detect is eliminated.

The possibility of smaller aggregates containing more than two porphyrin monomers has also been considered. The presence of such extended aggregates can be eliminated on the

(17) (a) Abraham, R. J.; Bedford, G. R.; McNeillie, D.; Wright, B. *Org. Magn. Reson.* **1980**, *14*, 418−425. (b) Smith, K. M.; Bobe, F. W.; Goff, D. A.; Abraham, R. J. *J. Am. Chem. Soc.* **1986**, *108*, 1111−1120. (c) Abraham, R. J.; Smith, K. M. *J. Am. Chem. Soc.* **1983**, *105*, 5734−5741.

(18) (a) Fleisher, E. B.; Shachter A. M. *Inorg. Chem.* **1991**, *30*, 3763−3769. (b) Shachter, A. M. Coordinated and Linked Porphyrin Dimers, Trimers and Polymers. Ph.D. Dissertation, University of Colorado, Boulder, CO, 1989.

(19) (a) Eaton, S. S.; Eaton, G. R. *J. Chem. Soc., Chem. Commun.* **1974**, 576. (b) La Mar, G. N.; Eaton, G. R.; Holm, R. H.; Walker, F. A. *J. Am. Chem. Soc.* **1973**, *95*, 63.

basis of experimental ^{1}H NMR shifts and the relative intensities of the sharp β-pyrrole and phenyl proton resonances. All of the extended structures in Scheme 3 would have internal and terminal porphyrins in chemically distinct environments. These structures would be expected to give rise to sets of peaks for each environment. For example, the extended-stack structure would have the e′ and f′ protons and those of bridging 2-pyridyl substituents on internal porphyrins in the shielding zones of two adjacent porphyrin rings. The effects of two adjacent porphyrins would give rise to larger ring current shifts for the internal porphyrins. Stair-step structures derived from 3MeMg, 2PrMg, and 3BuMg would put the *meso*-15-phenyl ring and its para-alkyl substituent in the shielding zone of an adjacent porphyrin ring, thereby inducing a significant upfield shift of these resonances. The double-layer structure is highly unlikely as it would exhibit very high steric interaction energies due to crowding of the 5- and 15-meso substituents. Finally, both the stair-step and double-layer structures would have all g′ β-pyrrole protons, except for those on the terminal porphyrins in the shielding cones of neighboring porphyrins. All of these extended structures would be expected to give rise to additional resonances with chemical shifts and intensity ratios distinct from those of the dimers. None of these signatures are observed. Hence, ^{1}H NMR spectra of 10^{-4} M or greater 3MeMg, 3PrMg, and 3BuMg demonstrate that the dominant solution structure is dimeric and that this structure is stabilized by mutual coordination between the metal ion of one porphyrin and the *meso*-2-pyridyl substituent of a single partner porphyrin.

The propensity for dimerization of *meso*-2-pyridylporphyrins is further indicated in concentrated solutions of 4MeMg and 4BuMg, wherein each porphyrin contains two *meso*-2-pyridyl groups (on opposite sides of the porphyrin ring, Scheme 2). These solutions yield ^{1}H NMR spectra containing the same upfield signatures observed for $[3MeMg]_2$ and $[3BuMg]_2$. Specifically, resonances from protons of the coordinated *meso*-2-pyridyl group and the β-pyrrole protons appear upfield from the monomeric values at the same positions observed in $[3MeMg]_2$ and $[3BuMg]_2$. Furthermore, resonances of the second *meso*-2-pyridyl group appear near those of the corresponding monomers (data not shown). So, even though 4MeMg and 4BuMg both contain two 2-pyridyl substituents, only one of them is coordinated to another magnesium porphyrin. Hence, the energetically favored solution structure of these magnesium bis-2-pyridylporphyrins in concentrated solution is also dimeric with one *meso*-2-pyridyl group coordinated to the magnesium center of the partner porphyrin.

UV−Visible Absorption Spectroscopy of the Dimers. Table 2 lists the absorption maxima for several monomeric and dimeric magnesium tetraarylporphyrins. Differences in the UV−visible absorption spectra of monomeric and dimeric magnesium 2-pyridylporphyrins allow tracking and quantitation of the concentration-dependent interchange between them. Changes in the absorption spectrum that are associated with this interconversion ($3BuMg \rightleftharpoons [3BuMg]_2$) are seen in Figure 2. Each successive spectrum was obtained from a solution having a 10-fold decrease in concentration and a 10-fold increase in the optical path length through the sample. The spectra in Figure 2 exhibit a split B (or Soret) band at the highest concentration with B′(0,0) and B″(0,0) occurring at 429 and 414 nm, respectively ($\Delta\nu = 845$ cm^{-1}). Similar B-band splitting has been observed for most complexes in this class[6] and is attributed to excitonic interaction between the large Soret transition dipoles of the constituent porphyrin chromophores. The shape of the B-band envelope in spectrum A of Figure 2 is

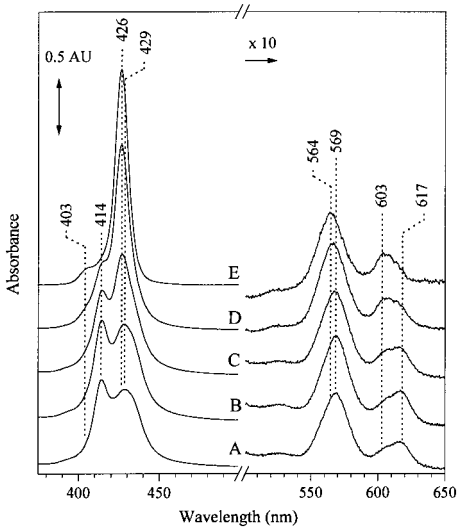

Figure 2. UV−visible spectra of 3BuMg in CH_2Cl_2 acquired under the following conditions: (A) 4.35×10^{-4} M total porphyrin, 0.1-mm path length; (B) 4.35×10^{-5} M, 1.0-mm path length; (C) 4.35×10^{-6} M, 10-mm path length; (D) 4.35×10^{-7} M, 100-mm path length; (E) [D − (0.7 × A)] to show the features of the pure four-coordinate Mg 2-pyridylporphyrinate.

similar to that of analogous Zn complexes,[6b] suggesting that these spectral features are characteristic of the mutually coordinated dimers of the normal metalloporphyrins.

Spectrum A of Figure 2 also reveals multiplicity in the Q(0,0) band, with Q′(0,0) and Q″(0,0) at 617 and 603 nm, respectively. A 10-fold increase in concentration did not cause a measurable change in the Q-band region of the spectrum. The insensitivity of the 617/603-nm band intensity ratio to changes in concentration between 10^{-4} and 10^{-3} M $[3BuMg]_2$ may be rationalized in a number of ways. First, the 603- and 617-nm bands could arise from either excitonic interaction between the two magnesium porphyrins ($\Delta\nu = 350$ cm^{-1}) or intradimer charge resonance.[7] Although both Q exciton bands would be allowed (both B-band components are observed), splitting seems unlikely; it is unprecedented in porphyrin dimers of this type[6] due to weak coupling of the small Q transition dipoles in normal porphyrins. The possibility of charge resonance[7] cannot be eliminated. A second possibility is that two Q-bands are a consequence of symmetry lowering in the dimer. However, this seems unlikely, as there is no apparent splitting of the Q(0,1) band. The third possibility is that the 603-nm band arises from the presence of a monomer, which has its Q-band at 603 nm. Since the amount of monomer should diminish with increasing concentration, the 603-nm band should lose intensity with increasing Mg(2-pyridylporphyrin) concentration. Since no intensity loss is observed with a 10-fold increase in concentration, it is unlikely that the 603-nm band arises from monomer in equilibrium with dimer. Since it is possible that the monomer could be generated by protonation of the 2-pyridyl nitrogen atom, a solution of the dimer was treated with anhydrous Na_2CO_3 to test whether the base would diminish the 603-nm band; the spectrum was unchanged. Moreover, neither NMR nor TLC analysis revealed the presence of free-base porphyrin. All evidence indicates that the 603-nm band is characteristic of the dimer. Finally, it is possible that the 603-nm band is due to a singly linked dimer (sd) that exists in a constant ratio with the mutually coordinated (md) dimer. This is corroborated by a smaller monomer-like Q-band in the spectrum of the *meso*-2-imidazolyl[20] analogue of $[3PrMg]_2$. Because this complex is linked by mutual coordination through two five-membered

Scheme 4

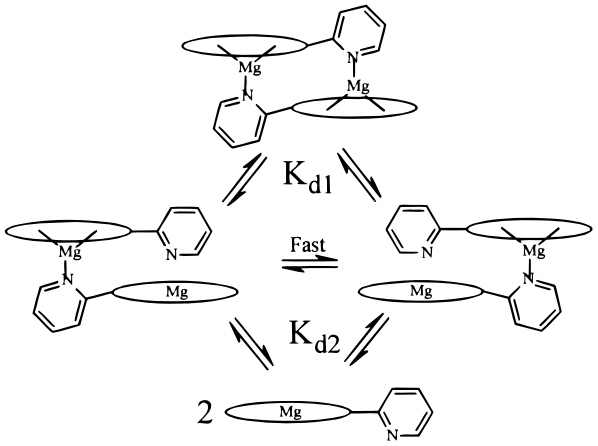

imidazole rings, the distortion required to bring the nitrogen lone pair of electrons into the proper orientation for coordination is expected to be less than that for the 2-pyridyl analogues $[3MeMg]_2$, $[3PrMg]_2$, and $[3BuMg]_2$. Consequently, the *meso*-2-imidazolyl dimer is considerably more stable (still mostly dimerized at 10^{-7} M) than the dimers linked by 2-pyridyl groups. This stability is consistent with a lower population of singly linked dimers. Evidence for the sd model is that sd and md (a) occur in constant ratio (UV−visible spectra) and (b) account for all of the porphyrin (evidenced by ^{1}H NMR). The observation of a single sharp NMR spectrum requires that they are either in rapid exchange or indistinguishable by NMR (or both). Low-temperature NMR spectra of $[3PrMg]_2$ (−50 °C) show no significant temperature-induced shifts, which further requires that interchange between the top three species in Scheme 4 be rapid at temperatures down to −50 °C. Hence, it is proposed that multiplicity in the Q-bands is due either to an equilibrium mixture of sd and md, as illustrated in Scheme 4, or to an intradimer charge resonance transition in md.

There is no detectable change in the integrated B-band intensity and an approximately 10% increase in Q-band intensity upon converting the mutually coordinated dimers to monomeric five-coordinate pyridine adducts. Thus, the cofacial structure has minimal impact on the total absorption cross section of the porphyrin.

Fluorescence Spectroscopy of the Dimers. The monomeric compounds reported here have emission spectra similar to those of other magnesium porphyrins.[21] As expected based on the red shifts of the dimer B- and Q-bands (Table 2), S_1 and S_2 emissions from the dimers are shifted to lower energy than their monomer counterparts (665 → 670 nm and 446 → 467 nm, respectively). At porphyrin concentrations near 10^{-4} M, where dimers are the dominant species, the fluorescence quantum yield (Φ_f) of $[3MeMg]_2$ is diminished relative to that for 2MeMg in solutions of the same total magnesium porphyrin concentration. The data in Figure 3 show that Φ_f decreases with concentration for both complexes. Since high concentration favors cofacial aggregation even for porphyrins that do not contain coordinating substitutents,[17c,22] the decrease in Φ_f for concentrated porphyrins is consistent with literature precedence for diminished fluorescence in closely spaced cofacial porphyrin[23] and phthalocyanine aggregates.[24] Comparison of the curves in Figure 3 reveals a steeper decrease in Φ_f for 3MeMg than for 2MeMg. The mechanisms for nonradiative decay of S_1 that rely on diffusional encounters with other chromophores in unlinked porphyrins are more efficient for 3MeMg, in which the chromophores are *held* in close proximity by mutual coordination through their peripheral *meso*-2-pyridyl substituents.

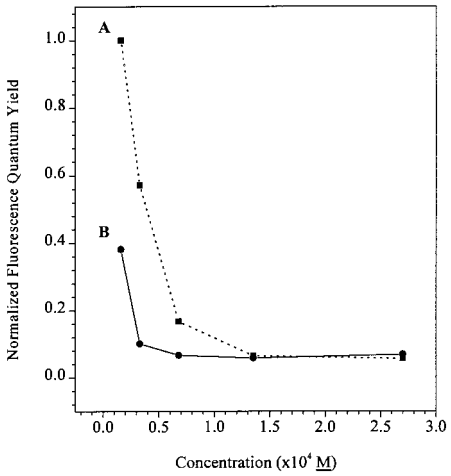

Figure 3. Relative fluorescence quantum yields in isomolar solutions of 2MeMg and 3MeMg: (A) 2MeMg, integrated intensity measurements for the fluorescence peak at 665 nm; (B) 3MeMg, integrated intensity measurements for the fluorescence peak at 670 nm.

Interconversion between Monomers and Dimers. The stepwise dissociation reactions of $[3MeMg]_2$, $[3PrMg]_2$, and $[3BuMg]_2$ are illustrated in Scheme 4. The stability of the dimer toward dissociation can be estimated from the dilution data in Figure 2. Specifically, the fraction of spectrum A in Figure 2 that must be subtracted from spectrum D to produce spectrum E [E = D − (0.35 × A)], which is characteristic of monomeric 2MeMg (MgTTP) and 2BuMg, provided an estimate of the fraction of the porphyrins that remained in the dimeric forms. This analysis shows that, at a concentration of 4.35×10^{-7} M porphyrin, 35% remained dimerized and yielded a value of 1.1×10^{-6} M for the overall dissociation constant, K_D. This estimate is based on the assumption that, under equilibrium conditions, the population of sd is too low to be observed.

Even if the sd model is accurate, the spectroscopic signatures of sd and md are expected to be very similar, making reliable dissection of the overall dissociation constant into its two components difficult. Nevertheless, within the sd model, the stepwise dissociation constants, K_{d1} and K_{d2}, have been estimated by two methods. The first is based on the relative intensities of the 603- and 617-nm bands obtained from peak-fitting the Q-band region of spectrum A in Figure 2. Assuming that the 603-nm band arises from the square planar half of sd, K_{d1} was estimated to be 1.3. The value for K_{d2} was estimated from changes in the absorbance spectra that occur upon dilution. As described above, at a concentration of 4.35×10^{-7} M porphyrin, 35% of the porphyrin would be in the md and sd forms. This analysis yields a value of 1.9×10^{-6} M for K_{d2}. The overall K_D calculated from K_{d1} and K_{d2} (their product) is 2.6×10^{-6}

(20) Viswanathan, A.; Rodgers, K. R. Details to be published in a full report.
(21) Gradyushko, A. T.; Tsvirko, M. P. *Opt. Spektrosk.* **1971**, *31*, 548 (English translation: *Opt. Spectrosc.* **1971**, *31*, 291).
(22) Stelmakh, G. F.; Tsvirko, M. P. In *Porphyrins, Excited States and Dynamics*; Gouterman, M., Rentzepis, P. M., Straub, K. D., Eds.; American Chemical Society: Washington, DC, 1986; Vol. 321, Chapter 8.
(23) (a) Chang, C. K.; Kuo, M.-S.; Wang, C.-B. *J. Heterocycl. Chem.* **1977**, *14*, 1285−1288. (b) Eaton, S.; Eaton, G. R.; Chang, C. K. *J. Am. Chem. Soc.* **1985**, *107*, 3177. (c) Collman, J. P.; Chong, A. O.; Jameson, G. B.; Oakley, R. T.; Rose, E.; Schmittou, E. R.; Ibers, J. A. *J. Am. Chem. Soc.* **1981**, *103*, 516.
(24) Moser, F. H.; Thomas, A. L. *Phthallocyanine Compounds*; ACS Series 157; Reinhold Publishing: New York, 1963.

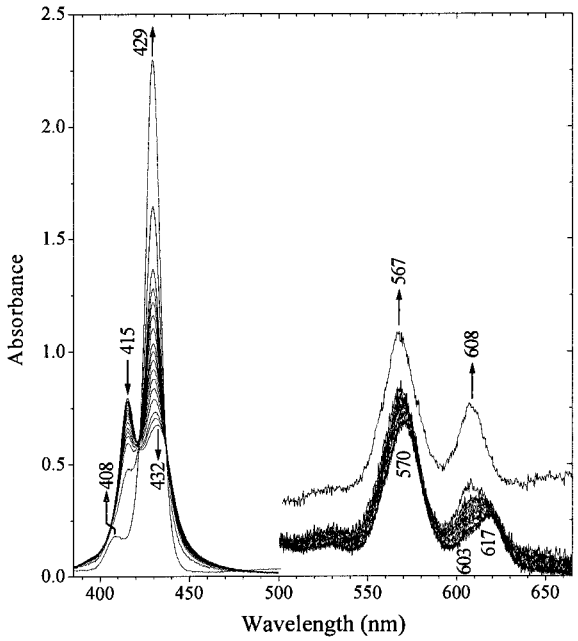

Figure 4. Spectra from the UV−visible spectrophotometric titration of 3PrMg with pyridine in CH_2Cl_2. Spectra were acquired with a 1.0-mm path length cell at 290 K. [Py]/[3PrMg] ranged from 0 to 60. Absorbance scale of each spectrum has been adjusted for dilution due to addition of the pyridine titrant solution.

M. Similar values of 2.4, 7.8×10^{-7} M, and 1.9×10^{-6} M (for K_{d1}, K_{d2}, and K_D, respectively) were derived by submitting the same data (Figure 2) to an evolving factor analysis. The overall dissociation constants obtained for both models differ by less than an order of magnitude and correspond to an overall stability constant, β_2, between 3.8×10^5 M^{-1} and 9.1×10^5 M^{-1}.

Disaggregation by Exogenous Ligands. Upon treatment of $[3MeMg]_2$ and $[3BuMg]_2$ with DMSO, DMF, acetone, or pyridine, the dimeric absorption signatures were lost at the expense of sharp spectra characteristic of monomeric magnesium tetraarylporphyrins. In the case of pyridine, spectra identical to those of 2MeMg(Py) and 2BuMg(Py) were observed. This is seen for pyridine by changes in the B-band region of the absorbance spectrum in Figure 4. Disaggregation of the dimeric magnesium complexes was investigated by ^{1}H NMR titration of $[3MeMg]_2$, $[3PrMg]_2$, and $[3BuMg]_2$ with pyridine-d_5 as a competing ligand. Proton NMR monitoring of the $[3PrMg]_2$ titration yielded the series of spectra shown in Figure 5. As the mole fraction of pyridine was increased, the peaks attributed to dimeric porphyrins decreased in intensity. Simultaneously, new signals appeared near their monomer positions and grew in integrated intensity as they shifted toward frequencies characteristic of the monomer spectrum. Qualitatively, the stability of the dimer is evidenced by the large pyridine/$[3PrMg]_2$ mole ratio required for complete disaggregation of the dimer. Even in the presence of a 60-fold excess of pyridine, several percent of the porphyrin persists in the dimerized forms. The stabilities of MgTPP(py) (4.27×10^3 M)[25] and 2MeMg(py) (MgTTP-(py)) are much greater than those of the 3MeMg−, 3PrMg−, and 3BuMg−pyridine adducts. This is seen by ^{1}H NMR titration of 2MeMg with pyridine-d_5. A plot of line width for the *o*-tolyl proton versus equivalents of pyridine added decreases sharply between 0 and 1 equiv and levels off without measurable change between 1 and 6 equiv (Supporting Information, Figure S7). This suggests an approximately stoichiometric addition of one pyridine ligand per Mg^{2+} center, when there is no competition from the *meso*-2-pyridyl groups of other porphyrins. As seen in Figure 5, addition of 1 equiv of pyridine to $[3PrMg]_2$ barely causes a discernible change in the NMR spectrum. Similarly, only subtle changes are observed in the absorption spectrum at low pyridine/$[3PrMg]_2$ ratios. The quantitative data used to determine the equilibrium constant for this reaction were extracted from the NMR spectra in Figure 5 by integrating the e′ (β-pyrrole) proton resonance for each pyridine addition and using them to construct the Scatchard plot[26] in Figure 6. These resonances are well suited for quantitative analysis, as they arise from a single chemical environment; they are sharp, and they are well separated from other signals.

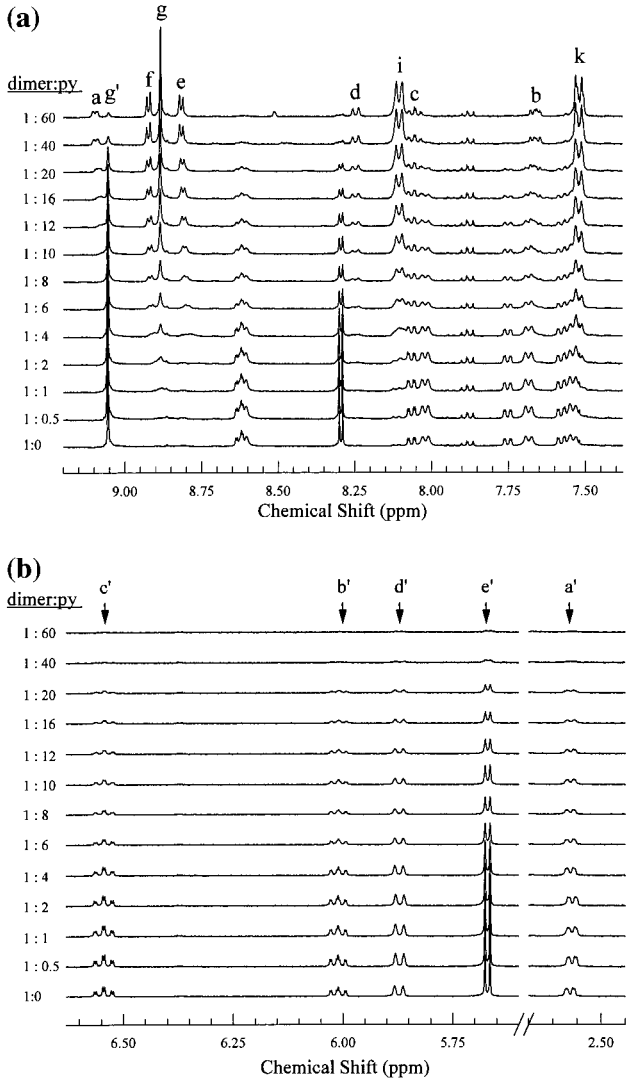

Figure 5. Data from the ^{1}H NMR titration of 1.37×10^{-3} M $[3PrMg]_2$ with pyridine-d_5 in $CDCl_3$ at 293 K. The $[3PrMg]_2$/py mole ratios are indicated to the right of the corresponding spectra. (A) Aromatic region showing [py]-dependent shifts of average peaks (dotted lines) due to the rapid equilibrium between monomer and sd. (B) Upfield region showing ring-current-shifted pyridyl and β-pyrrole proton signals. Assignments are based on the COSY map of $[3BuMg]_2$ (see Supporting Information).

The macroscopic equilibrium constants, K_1 and K_2 (Scheme 5), are related to the microscopic equilibrium constant, *k*, obtained from the Scatchard plot, by statistical factors of 1/2

(25) Kadish, K. M.; Shiue, L. R. *Inorg. Chem.* **1982**, *21*, 1112−1115.

(26) Edsall, I. T.; Gutfreund, H. *Biothermodinamics: The Study of Biochemical Processes at Equilibrium*; Wiley: New York, 1983.

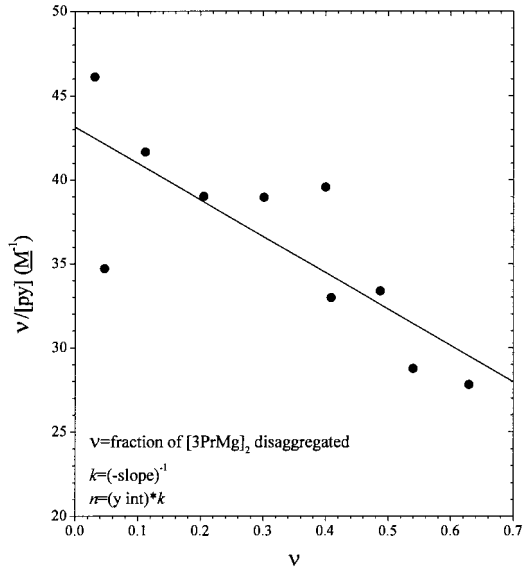

Figure 6. Scatchard plot based on e′ β-pyrrole ^{1}H NMR intensity as a function of added pyridine. The solid line was determined by linear least-squares analysis; $y = (21.7 \pm 5.9)x + (43.1 \pm 2.2)$. Binding parameters are listed in Table 3.

Scheme 5

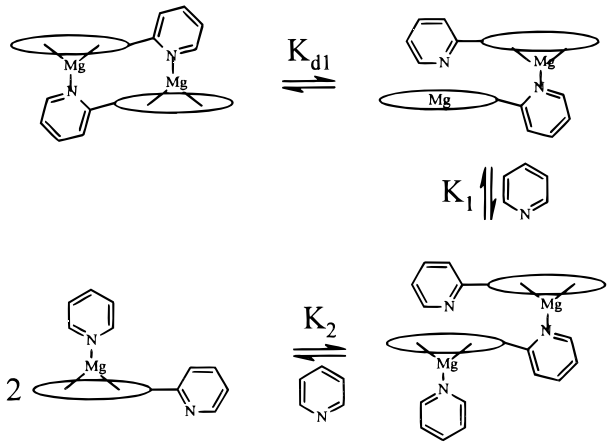

Table 3. Binding Parameters Obtained from Scatchard Analysis of the Data from Titrations of $[3PrMg]_2$ with Pyridine

$10^2 \times k^a$ (M)	n	$10^2 \times K_1{}^b$ (M)	$10^2 \times K_2{}^c$ (M)	$10^3 \times K_{total}{}^d$ (M^2)	ΔG_{total} (kJ/mol)
4.5 ± 1.2	2.0 ± 0.5	2.3 ± 0.6	9.0 ± 2.4	2.1 ± 0.8	15.0

[a] $k = -(\text{slope})^{-1}$ from Scatchard plot. [b] $K_1 = (1/2)k$. [c] $K_2 = 2k$. [d] $K_{total} = K_1 \times K_2$.

and 2, respectively.[26] These Scatchard parameters indicate that loss of the dimer NMR signature (upfield-shifted e′ and f′ β-pyrrole resonances) requires binding of two pyridine molecules (one per monomer) to independent binding sites. Binding parameters obtained from the pyridine titration experiment are listed in Table 3.

The spectra in Figure 5 reveal two key aspects of the interconversion between monomer and dimer. First, the unchanging chemical shifts and line widths of resonances from the dimer suggest that the cofacial structure is static on the NMR time scale. Second, the [pyridine]-dependent shift toward the monomer resonances as ligand saturation is approached suggests that a singly linked dimer and the monomeric pyridine adduct are in rapid exchange on the NMR time scale. These two distinguishable processes indicate that the pyridine-induced

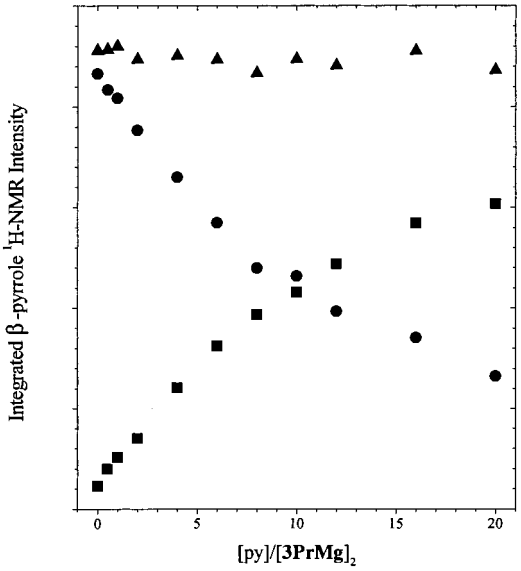

Figure 7. Plot of integrated β-pyrrole intensity of monomeric (squares) and dimeric (circles) complexes versus equivalents of pyridine added. Invariance of the total β-pyrrole intensity (triangles) as a function of added pyridine indicates mass balance between monomer and dimer throughout the titration.

disaggregation of the dimer must proceed by at least two steps. The plots in Figure 7 show that, when the β-pyrrole intensity from a dimer vanishes due to disaggregation by exogenous pyridine coordination, it is fully accounted for in the spectrum of the monomeric pyridine adduct. At any given [py], any porphyrin that is not in either the static cofacial or the monomeric form is less than the uncertainty in the NMR integration.

Basis of Dimer Stability. The dimeric metallo-2-pyridylporphyrins and bis-2-pyridylporphyrins add to a growing body of evidence for inherent stability of the dimeric edge-over-edge structure.[6,7] This evidence points to an intrinsic driving force for the formation of porphyrin and chlorin aggregates with this edge-over-edge structure, even without strongly coordinating peripheral substituents.[6i,j,17] In examples where monomers are not linked by metal−ligand bonds, the aggregates can be large.[6i,7j,k] For example, in aqueous porphyrin and metalloporphyrin aggregates whose formation is driven by addition of acid or salt, aggregates containing an average of 11 monomers have been demonstrated.[6i] However, when metalloporphyrin aggregation is driven by intermolecular metal−ligand bond formation, aggregate size depends on the nature of the linking substituent. In the molecules studied here and in several other members of this class,[6ab,27,28] bonding between the metal center of one porphyrin and the coordinating group of another imposes steric barriers to further aggregation by intermolecular coordination. Solution and solid-state structures of these complexes indicate that these constraints render any further intermolecular coordination other than mutual coordination unfavorable. The dominance of $[3PrMg]_2$ ^{1}H NMR signatures between −50 and 90 °C (spectrum acquired in bromoform) suggests that the dimers are the thermodynamically favored products of coordinative aggregation. However, the possibility that the dimers are kinetic products cannot be completely discounted.

(27) (a) Balch, A. L.; Latos-Grażyński, L.; Noll, B. C.; Olmstead, M. M.; Zovinka, E. P. *Inorg. Chem.* **1992**, *31*, 2248−2255. (b) Balch, A. L.; Noll, B. C.; Olmstead, M. M.; Reid, S. M. *J. Chem. Soc., Chem. Commun.* **1993**, 1088−1090.

(28) (a) Goff, H. M.; Shimomura, E. T.; Lee, Y. J.; Sheidt, R. *Inorg. Chem.* **1984**, *23*, 315−321. (b) Godziella, G. M.; Tilotta, D.; Goff, H. M. *Inorg. Chem.* **1986**, *25*, 2142−2146.

Steric interactions between the porphyrin and substituents at the pyridine α carbon lower the stability of 2-substituted pyridines. For example, MgTPP(2-picoline) ($\beta_1 = 2.95 \times 10^2$ M^{-1}) is 14.5 times less stable than MgTPP(py) ($\beta_1 = 4.27 \times 10^3$ M^{-1}),[25] even though 2-picoline is more basic than pyridine.[29] The *meso*-2-pyridylporphyrin is also sterically hindered, and the electron-withdrawing nature of the porphyrin is expected to render the 2-pyridyl group less basic than pyridine ($pK_{a(pyridine)} = 5.29$; $pK_{a(2-phenylpyridine)} = 4.48$[29]). Insofar as the porphyrin is expected to diminish the pK_a of pyridine in a manner analogous to that of a phenyl group, the contribution of σ-bonding to the stability of sd is expected to be smaller than that for a pyridine complex. Additionally, the porphyrin provides steric hindrance to formation of the Mg−(*meso*-2-pyridyl) bond, which is expected to further diminish the formation constant by at least 1.7 log units from that predicted on the basis of pK_a alone. The 1.7 log-unit offset was estimated from the offsets of 2-picoline and 2-aminopyridine from the linear free-energy line for binding of unhindered pyridine ligands to MgTPP.[25] This crude estimate leads to a predicted sd formation constant of approximately 75 M^{-1} ($\Delta G = -10.7$ kJ/mol). However, the estimated formation constant for sd is between 5.3×10^5 M^{-1} and 1.3×10^6 M^{-1} (K_{d2}^{-1}, -34.5 kJ/mol $\leq \Delta G \leq -32.3$ kJ/mol), which involves formation of the first Mg−(2-pyridyl) bridge. The estimated stability of sd is more than 20 kJ/mol greater than predicted solely upon the basis of Mg−(2-pyridyl) σ-bonding. This added stability may stem from the cofacial dimeric structures. Stability is gained from $\pi-\pi$ interaction between the metalloporphyrins.[30] This contribution to the stability of cofacial porphyrin and metalloporphyrin aggregates has been estimated to lie between −38 and −58 kJ/mol for tethered Zn porphyrin dimers. The tethers in these molecules allow optimal cofacial conformations, wherein a pyrrole ring of one metalloporphyrin lies directly over the metal center of its partner.[30] Since the extent and geometry of porphyrin overlap in sd and md are templated by 2-pyridyl coordination, the optimal overlap geometry is precluded. Hence, the contribution of $\pi-\pi$ interaction to the stabilities of sd and md may be smaller than that reported for tethered Zn porphyrin dimers and may explain the smaller $\pi-\pi$ contribution in the systems reported here.[30] Additional stability results from a chelate effect that arises from the diminished entropic cost for formation of the second Mg^{2+}−(2-pyridyl) bond.

Control of Aggregate Size by the Chelate Effect. The notion of chelate effects on the stabilities of md and sd is further supported by reports from recent studies of Fe(III), Mn(III), and Ga(III) hyrdroxytetraphenylporphyrins.[31] These complexes are shown to form mutually coordinated (cyclic) trimers in both the solution (Fe, Mn, and Ga)[31] and solid (Fe)[31d] states. Mutually coordinated dimeric structures are precluded in these complexes due to unfavorable steric interactions involving their *meso*-phenyl substituents. Even though there is no obvious steric barrier to formation of linear oligomers or polymers, the favored products are the cyclic trimers. As suggested above for the 2-pyridyl bridged dimers, the propensity to close a three-monomer ring over continued linear growth may also be entropically driven by the chelate effect. Hence, studies of dimers and trimers suggests that formation of the smallest possible mutually coordinated cyclic aggregate is energetically favored.

The dimers reported here differ fundamentally from aggregates formed with zinc *meso*-4-pyridylporphyrins, which have been shown to form extended singly linked aggregates by coordination of the nitrogen atom of a *meso*-4-pyridyl substituent to the Zn center of an adjacent porphyrin.[18] Orientation of the pyridyl nitrogen in these complexes precludes mutual coordination to form a dimeric structure. Single-crystal X-ray data show that the porphyrin planes of adjacent monomer units are approximately orthogonal and, consequently, do not exhibit strong excitonic interaction between the constituent chromophores.[18] These 4-pyridyl aggregates are clearly linear in the solid state.[18] Moreover, the average molecular weight in solution corresponds to that of a trimer. Since a tetramer would be required to form a cyclic aggregate, it was either not observed or was part of a mixture in which it could not be identified. The cyclic tetramer has recently been identified by low-temperature NMR, and a cyclic tetramer of ruthenium 4-pyridyltristolylporphyrin has also been characterized.[32] Consistent with the chelate-effect model, this class of compounds also favors formation of the smallest cyclic aggregate at low temperatures.

When the structure of the coordinating substituent is such that four or more monomers are required to form a mutually coordinated cyclic aggregate, the conformational degrees of freedom that govern relative porphyrin orientations become large. The result of such conformational freedom may be that the rate of linear growth can compete effectively with the rate of ring closure. Linear oligomers may be kinetically favored, even though the closed structures are thermodynamically favored. Hence, it may become difficult to observe the closed aggregates due to kinetic stability of higher molecular-weight linear oligomers and polymers. In such cases, the chains may grow until they precipitate out of solution. We have observed this behavior with Zn[(3-py)Tr(4-*n*-Bu)PP], which forms one or more aggregates with very low solubility in noncoordinating solvents.

Conclusion

The synthesis and characterization of three new mutually coordinated magnesium 2-pyridylporphyrin dimers has been described. These dimers exhibit cofacial edge-over-edge structures, having their porphyrin π systems in close proximity, as evidenced by the excitonic coupling of the constituent chromophores and diagnostic chemical shift patterns. These complexes are quite stable, having overall formation constants of approximately 5×10^5 M^{-1}. The cofacial structures likely exist as singly and mutually coordinated complexes under ambient conditions.

Acknowledgment. This work was funded by AFOSR/BMDO (Award No. F49620-96-1-0359).

Supporting Information Available: One- and two-dimensional NMR data for ligands and complexes (Figures S1−S6), *o*-tollyl ^1H NMR line width plotted as a function of [Py]/[Mg(TTP)] (Figure S7) (8 pages). Ordering information is given on any current masthead page.

IC971421T

(29) Schoefield, K. S. *Hetero-Aromatic Nitrogen Compounds*; Plenum Press: New York, 1967; p 146.

(30) (a) Hunter, C. A.; Sanders, J. K. M. *J. Am. Chem. Soc.* **1990**, *112*, 5525−5534. (b) Hunter, C. A.; Meah, M. N.; Sanders, J. K. M. *J. Am. Chem. Soc.* **1990**, *112*, 5773−5780. (c) Anderson, H. L.; Hunter, C. A.; Meah, M. N.; Sanders, J. K. M. *J. Am. Chem. Soc.* **1990**, *112*, 5780−5789.

(31) (a) Wojaczyński, J.; Latos-Grażyński, L. *Inorg. Chem.* **1995**, *34*, 1044−1053. (b) Wojaczyński, J.; Latos-Grażyński, L. *Inorg. Chem.* **1995**, *34*, 1054−1062. (c) Wojaczyński, J.; Latos-Grażyński, L. *Inorg. Chem.* **1996**, *35*, 4812−4818. (d) Wojaczyński, J.; Latos-Grażyński, L.; Olmstead, M. M.; Balch, A. L. *Inorg. Chem.* **1997**, *36*, 4548−4554.

(32) Funatsu, K.; Imamura, T.; Ichimura, A.; Sasaki, Y. *Inorg. Chem.* **1998**, *37*, 1798−1804.

(33) Edwards, L.; Dolphin, D. H.; Goutermann, M.; Adler, A. D. *J. Mol. Spectrosc.* **1971**, *38*, 16.